Adaptive Input–Output Feedback-Linearization-Based Torque Control of Synchronous Reluctance Motor Without Mechanical Sensor

Hossein Abootorabi Zarchi, Jafar Soltani, and Gholamreza Arab Markadeh

***Abstract*—In this paper, a well-known adaptive input–output feedback-linearization (AIOFL) technique is used for speed and torque-tracking control of synchronous reluctance motor drive. This controller is capable of estimating motor two-axis inductances ($\mathbf{L_d}$, $\mathbf{L_q}$) simultaneously. The overall stability of the proposed control and the persistency of excitation condition are proved based on Lyapunov theory. In addition, the maximum rate of change of torque control scheme is applied to generate the motor d- and q-axis reference currents which are needed for AIOFL controllers. Another contribution of this paper is to estimate the rotor speed and position. For low-speed estimation, we have to eliminate the current and voltage sensors' dc offsets, detect the stator resistance, and take into account the voltage drop of the inverter power switches. We solve these problems by using a simple technique for eliminating the voltage sensors and a simple method for online estimation of the stator resistance and modeling the voltage drop of the inverter power switches. It is worthwhile to mention that the current sensors' dc offsets, seen on the measured currents, are negligible. Finally, the validity of the proposed method is verified by experimental results.**

***Index Terms*—Adaptive input–output feedback linearization (AIOFL), encoderless, synchronous reluctance motor (SynRM).**

I. Introduction

THE synchronous reluctance motor (SynRM) is one of the oldest and simplest types of electric motors. In recent years, it has been shown that SynRM can be competitive with other ac motors [1]–[7]. A SynRM is superior to an induction motor due to the absence of rotor copper losses, to brushless motors due to inexpensive rotor structure, and to a switched reluctance motor because of a much lower torque ripple and low noise.

In the last two decades, the challenging task of SynRM parameter identification has been taken up by some researchers [8]–[11]. One may notice that uncertainties and variations of the parameters seriously affect the motor performance, in particular, its closed-loop control stability. In offline parameter-identification methods described in [8] and [9], the SynRM electrical parameters are obtained for some operating points by practical test and inserted in lookup tables or mathematically approximated by some curves. An alternative solution is the online estimation of the machine parameters. In [10] and [11], d- and q-axis inductances and stator resistance ($\mathbf{L_d}$, $\mathbf{L_q}$, $\mathbf{R_s}$) are estimated using a recursive least squares (RLS) estimator (RLSE). It is not necessary to say that the RLSE, at each step of time, needs to reset a so-called positive definite covariance matrix which results in a high computation storage and time [12]. Betz *et al.* [10] have also described in their paper that, although it is possible to estimate all the electrical machine parameters by the RLS method, the estimator performance is considerably improved if only $\mathbf{L_d}$ is estimated with assumption of constant $\mathbf{R_s}$ and $\mathbf{L_q}$.

In [11], three parallel nonlinear observers are used to estimate the SynRM rotor speed, rotor position, and the motor electrical parameters ($\mathbf{L_d}$, $\mathbf{L_q}$, $\mathbf{R_s}$). In this method, a so-called extended electromotive force (EEMF) vector is introduced in a two-axis stationary reference frame with components of ($\hat{e}_{\mathrm{Ds}}$, $\hat{e}_{\mathrm{Qs}}$). These quantities can be online estimated if the rotor speed and machine parameters ($\mathbf{L_d}$, $\mathbf{L_q}$, $\mathbf{R_s}$) are estimated simultaneously. RLSE estimates the motor electrical parameters which are used by the EEMF observer as well as the motor controller. In this approach, the RLSE needs to know the motor estimated speed and measured currents and voltages. One may note that, in the method of [11], the rotor speed is estimated by derivation of an estimated angle of the rotor position which is the output of the EEMF observer. The overall stability of such a very complicated system is dubious and really cannot be analytically proved. As mentioned in [11], this method is incapable of parameter estimation in low speed; although Ichikawa *et al.* [11] have claimed that motor-speed estimation is possible above 50 r/min, however, there exists no practical results that can support this claim. The results given in [11] show the motor-speed estimation only from 500 to 1000 r/min. In [13], a predictive direct torque control has been presented for encoderless SynRM, which is able to operate at low speed. At low-speed operation, the rotor angular position is estimated by injecting test-voltage signals (TVSs) to detect the spatial orientations of existing position-dependent rotor anisotropies. However, the TVSs deteriorate the performance of the predictive algorithm, and they create some audible noise. In addition, the method in

Manuscript received November 12, 2008; revised June 16, 2009. First published July 7, 2009; current version published December 11, 2009.

H. Abootorabi Zarchi and J. Soltani are with the Faculty of Electrical and Computer Engineering, Isfahan University of Technology, Isfahan 84156-83111, Iran (e-mail: abootorabi9@yahoo.com; j1234sm@cc.iut.ac.ir).

G. Arab Markadeh is with the Department of Engineering, Shahrekord University, Shahrekord 88186-34141, Iran (e-mail: arab-gh@eng.sku.ac.ir).

Color versions of one or more of the figures in this paper are available online at http://ieeexplore.ieee.org.

Digital Object Identifier 10.1109/TIE.2009.2026379

[13] is complicated, and for each chosen motor, it is required to obtain the motor inductances by offline parameter identification methods.

The main contribution of this paper is to use the well-known adaptive input–output feedback-linearization (AIOFL) technique for SynRM torque control without using mechanical position and voltage sensors. The proposed controller is capable of simultaneous estimating of d- and q-axis inductances ($\mathbf{L_d}$, $\mathbf{L_q}$). The overall stability of this controller is analytically proved based on Lyapunov theory. In the proposed control technique, we need to know the motor d- and q-axis reference currents. These reference currents can be generated based on any chosen torque-control strategy for SynRM, such as maximum torque control, maximum power-factor control, maximum rate of change of torque control (MRCTC), or id constant strategy [7]–[10]. Based on [10], MRCTC is very sensitive to variations and uncertainties that usually exist in parameters ($\mathbf{L_d}$, $\mathbf{L_q}$). Therefore, in this paper, we chose an MRCTC strategy that requires the actual values of motor electrical parameters. Our control approach enables estimation of the motor speed. One may note that in the rotor low-speed estimation, we encounter problems such as voltage and current sensors' dc offsets, as well as the slow variation of stator resistance with temperature. We solve these problems by using a simple method for eliminating the voltage sensors and a simple method for an online estimation of the stator resistance by using a proportional–integral (PI) estimator and also modeling the voltage drop of the inverter power switches. It is worthwhile mentioning that the current sensors' dc offset seen on the measured currents is negligible.

II. SynRM Model

The SynRM d–q axis equations in the rotor reference frame, taking into account the cage winding, is given by [14]

$$v_{\rm ds} = R_s i_{\rm ds} + \frac{d\lambda_{\rm ds}}{dt} - \omega_e \lambda_{\rm qs} \tag{1}$$

$$v_{\rm qs} = R_s i_{\rm qs} + \frac{d\lambda_{\rm qs}}{dt} + \omega_e \lambda_{\rm ds} \tag{2}$$

$$0 = R_{\rm dr} i_{\rm dr} + \frac{d\lambda_{\rm dr}}{dt} \tag{3}$$

$$0 = R_{\rm qr} i_{\rm qr} + \frac{d\lambda_{\rm qr}}{dt} \tag{4}$$

with

$$\begin{aligned}
\lambda_{\rm qs} &= L_{\rm mq}(i_{\rm qs} + i_{\rm qr}) + L_{\rm ls} i_{\rm qs} \\
\lambda_{\rm qr} &= L_{\rm mq}(i_{qs} + i_{\rm qr}) + L_{\rm lqr} i_{\rm qr} \\
\lambda_{\rm ds} &= L_{\rm md}(i_{\rm ds} + i_{\rm dr}) + L_{\rm ls} i_{\rm ds} \\
\lambda_{\rm dr} &= L_{\rm md}(i_{\rm ds} + i_{\rm dr}) + L_{\rm ldr} i_{\rm dr} \\
L_d &= L_{\rm md} + L_{\rm ls} \\
L_q &= L_{\rm mq} + L_{\rm ls}
\end{aligned} \tag{5}$$

where $\lambda_{\rm ds}$ and $\lambda_{\rm qs}$ are stator linkage fluxes, $v_{\rm ds}$ and $v_{\rm qs}$ are stator voltages, $i_{\rm ds}$ and $i_{\rm qs}$ are stator currents, $i_{\rm dr}$ and $i_{\rm qr}$ are rotor currents, $L_{\rm md}$ and $L_{\rm mq}$ denote mutual inductances, $L_{\rm ls}$ is a stator leakage, $L_{\rm ldr}$ and $L_{\rm lqr}$ are rotor leakages, L_d and L_q are stator inductances, $R_{\rm dr}$ and $R_{\rm qr}$ are rotor resistances, which are all in d- and q-axis rotor reference frame. R_s is stator resistance, and ω_e is the rotor electrical angular velocity. From (1)–(5), the equivalent circuits of SynRM can be represented by Fig. 1. Also, the motor-generated torque is

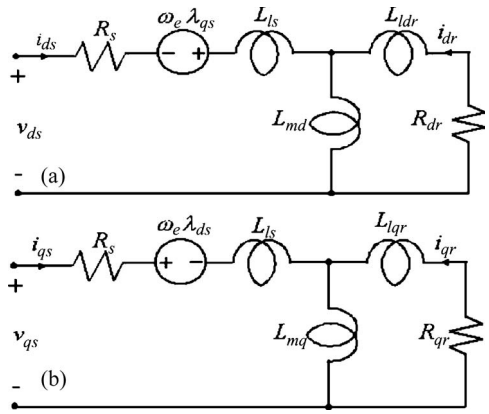

Fig. 1. Equivalent d–q axis circuits of the SynRM with cage. (a) d-axis equivalent circuit. (b) q-axis equivalent circuit.

$$\begin{aligned}
Te &= \frac{3}{2}\frac{P}{2}(\lambda_{\rm ds} i_{\rm qs} - \lambda_{\rm qs} i_{\rm ds}) \\
&= \frac{3}{2}\frac{P}{2}(L_d - L_q) i_{\rm ds} i_{\rm qs} + \frac{3}{2}\frac{P}{2}(L_{\rm md} i_{\rm dr} i_{\rm qr} - L_{\rm mq} i_{\rm qr} i_{\rm ds})
\end{aligned} \tag{6}$$

where P is the number of poles. In addition, the motor mechanical equations are

$$J_m \frac{d\omega_m}{dt} + B_m \omega_m = T_e - T_l, \qquad \frac{d\theta_m}{dt} = \omega_m \tag{7}$$

where J_m is the rotor moment of inertia, B_m is the friction coefficient, θ_m is the rotor displacement angle in mechanical degrees, ω_m is the rotor mechanical angular velocity, and T_l denotes the motor load torque.

III. AIOFL

Assuming the reference direct and quadrature axis fluxes defined by $\lambda^*_{\rm ds}$ and $\lambda^*_{\rm qs}$, the main aim is to apply the IOFL for SynRM drive system in order to obtain the reference space-voltage vector for space vector-pulsewidth modulation (SV-PWM) inverter which feeds the motor. For this purpose, ignoring the cage rotor of SynRM in Fig. 1 and choosing $\lambda_{\rm ds}$, $\lambda_{\rm qs}$, and ω_e as state variables and assuming $v_{\rm ds} = u_1$ and $v_{\rm qs} = u_2$ as the system control efforts, the nonlinear model is described by

$$\dot{X} = f(X) + g(X)U \tag{8}$$

where

$$\begin{aligned}
X &= [\, x_1 \quad x_2 \quad x_3 \,]^T = [\, \lambda_{\rm ds} \quad \lambda_{\rm qs} \quad \omega_e \,]^T \\
U &= [\, u_1 \quad u_2 \,]^T
\end{aligned} \tag{9}$$

$$f(X)=\begin{bmatrix} f_1 \\ f_2 \\ f_3 \end{bmatrix} = \begin{bmatrix} -R_s i_{\rm ds}+L_q i_{\rm qs}\omega_e \\ -R_s i_{\rm qs}-L_d i_{\rm ds}\omega_e \\ \left(\frac{3P}{4J_m}\left(\frac{1}{L_q}-\frac{1}{L_d}\right)\lambda_{\rm ds}\lambda_{\rm qs}-\frac{T_l}{J_m}\right)\Big/\frac{P}{2}-\frac{B_m\omega_e}{J_m} \end{bmatrix} \tag{10}$$

$$g(X)=[\,g_1 \quad g_2\,]=\begin{bmatrix} 1 & 0 \\ 0 & 1 \\ 0 & 0 \end{bmatrix}. \tag{11}$$

By introducing the following output variables:

$$y_1=\lambda_{\rm ds} \qquad y_2=\lambda_{\rm qs} \tag{12}$$

from (1), the system output dynamics can be obtained as

$$\begin{bmatrix} \dot y_1 \\ \dot y_2 \end{bmatrix}=\begin{bmatrix} f_1 \\ f_2 \end{bmatrix}+\begin{bmatrix} 1 & 0 \\ 0 & 1 \end{bmatrix}\begin{bmatrix} u_1 \\ u_2 \end{bmatrix}=\begin{bmatrix} f_1 \\ f_2 \end{bmatrix}+E(X)U. \tag{13}$$

From (8)–(13), an internal dynamics is recognized that its stability can be easily proved [12]. Based on the IOFL, the control effort is

$$U=E^{-1}\begin{bmatrix} v_1-f_1 \\ v_2-f_2 \end{bmatrix}. \tag{14}$$

Assuming the new state variables as

$$\dot y_1=v_1 \qquad \dot y_2=v_2. \tag{15}$$

The system control efforts are defined by

$$v_1=\frac{d\lambda^*_{\rm ds}}{dt}-\alpha_1 e_d=-R_s i_{\rm ds}+\omega_e L_q i_{\rm qs}+v_{\rm ds} \tag{16}$$

$$v_2=\frac{d\lambda^*_{\rm qs}}{dt}-\alpha_2 e_q=-R_s i_{\rm qs}-\omega_e L_d i_{\rm ds}+v_{\rm qs} \tag{17}$$

where α_1 and α_2 are positive constants, and $e_d=\lambda_{\rm ds}-\lambda^*_{\rm ds}$, $e_q=\lambda_{\rm qs}-\lambda^*_{\rm qs}$. Using (16) and (17), the motor estimated model is

$$v_1=\frac{d\lambda^*_{\rm ds}}{dt}-\alpha_1 e_d=-R_s i_{\rm ds}+\omega_e \hat a_2 i_{\rm qs}+v_{\rm ds} \tag{18}$$

$$v_2=\frac{d\lambda^*_{\rm qs}}{dt}-\alpha_2 e_q=-R_s i_{\rm qs}-\omega_e \hat a_1 i_{\rm ds}+v_{\rm qs} \tag{19}$$

where $\hat a_1=\hat L_d$ and $\hat a_2=\hat L_q$ are estimated values of L_d and L_q, respectively.

Linking (15), (18), and (19), the motor error dynamics are

$$\frac{de_d}{dt}=-\alpha_1 e_d \qquad \frac{de_q}{dt}=-\alpha_2 e_q. \tag{20}$$

This equation shows that for positive α_1 and α_2, e_d and e_q exponentially converge to zero.

IV. Adaptation Laws

Assume that

$$\widetilde a_1=a_1-\hat a_1 \qquad \widetilde a_2=a_2-\hat a_2 \tag{21}$$

where $\widetilde a_1$ and $\widetilde a_2$ are error values between actual and estimated parameters. From (13), (18), and (19), one can have

$$\begin{aligned} \dot\lambda_{\rm ds}&=(-R_s i_{\rm ds}+\omega_e L_q i_{\rm qs}+v_{\rm ds})-v_1+v_1 \\ &=\omega_e i_{\rm qs}\widetilde a_2+\dot\lambda^*_{\rm ds}-\alpha_1 e_d \\ \Rightarrow\quad \dot e_d&=\omega_e i_{\rm qs}\widetilde a_2-\alpha_1 e_d \end{aligned} \tag{22}$$

$$\begin{aligned} \dot\lambda_{\rm qs}&=(-R_s i_{\rm qs}-\omega_e L_d i_{\rm ds}+v_{\rm qs})-v_2+v_2 \\ &=-\omega_e i_{\rm ds}\widetilde a_1+\dot\lambda^*_{\rm qs}-\alpha_2 e_q \\ \Rightarrow\quad \dot e_q&=-\omega_e i_{\rm ds}\widetilde a_1-\alpha_2 e_q. \end{aligned} \tag{23}$$

Equations (22) and (23), in matrix compact form, become

$$\dot x=Ax+W^T\widetilde\theta \tag{24}$$

where $x=[e_d \quad e_q]^T$, $\widetilde\theta=[\widetilde a_1 \quad \widetilde a_2]^T$, and $A=\begin{bmatrix} -\alpha_1 & 0 \\ 0 & -\alpha_2 \end{bmatrix}$ with $W^T=\begin{pmatrix} 0 & \omega_e i_{\rm qs} \\ -\omega_e i_{\rm ds} & 0 \end{pmatrix}$.

The following Lyapunov function is used:

$$V=\frac{1}{2}x^Tx+\frac{1}{2}\widetilde\theta^T\Gamma^{-1}\widetilde\theta \tag{25}$$

where $\Gamma=\mathrm{diag}[\gamma_1,\gamma_2]$.

γ_1 and γ_2 are positive adaptation gains.

Derivation of V with respect to time t yields

$$\dot V=x^TAx+\widetilde\theta^TWx+\widetilde\theta^T\Gamma^{-1}\dot{\widetilde\theta}. \tag{26}$$

Assume the following adaptation law:

$$\dot{\widetilde\theta}=-\Gamma Wx. \tag{27}$$

Then, (26) is changed into

$$\dot V=x^TAx. \tag{28}$$

Since A is a negative definite matrix, therefore, from (28),

$$\dot V\le 0. \tag{29}$$

L_d and L_q are assumed to be unknown constant parameters, hence,

$$\dot{\widetilde a}_1=-\dot{\hat a}_1 \qquad \dot{\widetilde a}_2=-\dot{\hat a}_2. \tag{30}$$

As a result, from (27), the adaptation laws are obtained as

$$\dot{\hat a}_1=-\gamma_1\omega_e i_{\rm ds}e_q \tag{31}$$

$$\dot{\hat a}_2=\gamma_2\omega_e i_{\rm qs}e_d. \tag{32}$$

One may note that V is a radially unbounded function; therefore, (25) and (29) guarantee that e_d and e_q are bounded. As a result, from (24), W^T and $\dot x$ are bounded, too. From Barbalat's lemma [12], we obtain

$$\lim e_d=0 \quad \lim e_q=0 \qquad \text{for} \quad t\to\infty. \tag{33}$$

Moreover, if there exist two positive real constants T and C such that the persistency of excitation (PE) condition

$$\int_{t}^{t+T} W(\tau)W^T(\tau)d\tau \geq CI_2, \qquad \text{for all } t \geq 0 \tag{34}$$

is satisfied; then, from [12], it follows that the estimation error vector $\widetilde{\theta}$ exponentially converges to zero. It means that $\hat{L}_d$ and $\hat{L}_q$ finally reach their actual values.

For $\omega_e = 0$, we get

$$\int_{t}^{t+T} W(\tau)W^T(\tau)d\tau = \int_{t}^{t+T} \begin{pmatrix} 0 & 0 \\ 0 & 0 \end{pmatrix} d\tau.$$

Hence, the matrix in (34) is positive semidefinite, and the PE condition fails. For $\omega_e \neq 0$, the following result is obtained:

$$\int_{t}^{t+T} W(\tau)W^T(\tau)d\tau = \int_{t}^{t+T} \begin{pmatrix} \omega_e^2 i_{\mathrm{ds}}^2 & 0 \\ 0 & \omega_e^2 i_{\mathrm{qs}}^2 \end{pmatrix} d\tau = \int_{t}^{t+T} M(\tau)d\tau.$$

Since M is positive definite, the matrix in (34) is also positive definite. Hence, the PE condition is satisfied, and consequently, $\widetilde{\theta}$ asymptotically converges to zero.

V. SynRM MRCTC Strategy

In order to use the adaptive nonlinear controller described in the previous part, it is required to obtain the desired d- and q-axis reference currents. These reference currents are obtained in sinusoidal steady-state operating condition, considering the different control strategies relating to this motor as described in [17]–[20]. One may note that, in a sinusoidal steady-state condition, no currents are induced in the rotor cage, and hence, there is no need to take the cage windings into account in order to obtain the reference currents. Under this condition, the motor torque is given by [20]

$$T_e = \frac{3}{4}\frac{P}{2}(L_d - L_q)i_s^2 \sin(2\varepsilon) = K_t i_s^2 \sin(2\varepsilon) \tag{35}$$

where ε is the angle of the stator current vector i_s with respect to the rotor d-axis.

In [19], a novel method was presented by Chiba and Fukao for MRCTC of SynRM drive systems. It was found out that, to achieve the MRCTC, the machine should operate with the current vector at a constant angle of $\varepsilon_\psi = \tan^{-1}(L_d/L_q)$ or $\lambda_{\mathrm{ds}} = \lambda_{\mathrm{qs}}$. In [19], it is also proved that, for a given rotor speed and motor torque, the control method of MRCTC, compared with other torque-control strategies corresponding to SynRM, needs the minimum terminal voltage, and, as a result, a minimum rated voltage of the PWM inverter. This leads to the conclusion that, for the MRCTC strategy, a limitation may exist for motor terminal voltage from a viewpoint of PWM inverter dc-link voltage. In our proposed control scheme, we consider a limitation level for the magnitude of the stator reference flux up to a nominal value, i.e.,

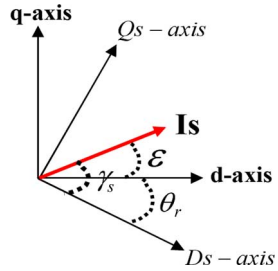

Fig. 2. Coordinates of SynRMs.

$$\begin{aligned} \lambda_{s,\mathrm{Max}}^* &= \sqrt{\lambda_{\mathrm{ds,Max}}^{*2} + \lambda_{\mathrm{qs,Max}}^{*2}} \\ \lambda_{s,\mathrm{Max}}^* &\overset{\mathrm{MRCTC}}{=} \sqrt{2}\lambda_{\mathrm{ds,Max}}^* = \sqrt{2}\lambda_{\mathrm{qs,Max}}^* \\ &= \lambda_{s,\mathrm{nominal}} \\ \Rightarrow \quad \lambda_{\mathrm{ds,Max}}^* &= \lambda_{\mathrm{qs,Max}}^* = \lambda_{s,\mathrm{nominal}}/\sqrt{2} \\ &= \lambda_{s,\mathrm{nominal,\,rms}}. \end{aligned} \tag{36}$$

Incorporating the aforementioned limitation ensures that the SV-PWM inverter always operates in its linear operating region determined by the corresponding SV-PWM scheme.

According to Betz *et al.* [10], MRCTC is very sensitive to the value of $\xi = L_d/L_q$ so that this parameter needs to be approximately determined with an accuracy of $\pm 10\%$.

VI. SynRM Rotor-Speed Estimation

Referring to Fig. 2, the rotor position angle is

$$\theta_r = \gamma_s - \varepsilon \tag{37}$$

where γ_s is the angle of the stator current vector, with respect to the direct axis of stationary reference frame, and ε is the angle of the stator current vector with respect to the rotor d-axis, which can be obtained from (35) by calculating the motor torque

$$T_e = \frac{3P}{4}(\hat{\lambda}_{\mathrm{Ds}} i_{\mathrm{Qs}} - \hat{\lambda}_{\mathrm{Qs}} i_{\mathrm{Ds}}) \tag{38}$$

where $\hat{\lambda}_{\mathrm{Ds}}$ and $\hat{\lambda}_{\mathrm{Qs}}$ are the estimated stator-flux components in stationary reference frame ($\mathbf{D_s}$,$\mathbf{Q_s}$) which are obtained by integrating the following equations:

$$\frac{d\hat{\lambda}_{\mathrm{Ds}}}{dt} = -\hat{R}_s i_{\mathrm{Ds}} + v_{\mathrm{Ds}} \tag{39}$$

$$\frac{d\hat{\lambda}_{\mathrm{Qs}}}{dt} = -\hat{R}_s i_{\mathrm{Qs}} + v_{\mathrm{Qs}} \tag{40}$$

where $\hat{R}_s$ is the estimated stator resistance, and $(i_{\mathrm{Ds}}, i_{\mathrm{Qs}})$ and $(v_{\mathrm{Ds}}, v_{\mathrm{Qs}})$ are the $\mathbf{D_s}$- and $\mathbf{Q_s}$-axis stator currents and voltages. A first-order low-pass filter is used in order to obtain a smoothing signal for the rotor position. Having estimated the angle of the rotor position $\hat{\theta}_r$, the rotor speed is calculated as follows:

$$\hat{\omega}_r = d\hat{\theta}_r/dt. \tag{41}$$

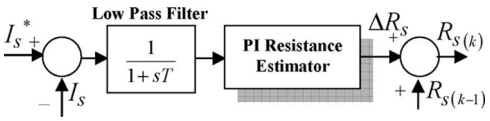

Fig. 3. PI resistance estimator of SynRM drive system.

One may note that, in the rotor low-speed estimation, we have some problems such as sensor dc offsets, the slow variation of stator resistance with temperature, and the voltage drop of the inverter power switches. We solve these problems in the next sections.

VII. Stator-Resistance Estimation

Among the machine variables, the estimated stator-flux vector is highly affected by the resistance changes, particularly at low speed. In addition, the IOFL controller can be made more reliable if the stator resistance is estimated online during the operation of the machine. In this paper, a PI estimator is employed based on comparing the actual and the reference currents to predict the stator resistance [15], [16]. As shown in Fig. 3, the error in the stator current is used as an input to the PI estimator. The technique is based on the principle that the error between the actual stator current and the reference current is proportional to the stator-resistance change [15]. The PI resistance estimator is described by

$$\Delta R_s = \left(K_P + \frac{K_I}{s}\right) \Delta I_s \tag{42}$$

where s is the Laplace operator and K_P and K_I are the proportional and integral gains of the PI estimator, respectively. The error between the actual stator current and its reference is passed through a low-pass filter with a very low cutoff frequency in order to attenuate the high-frequency component contained in the estimated stator current. Then, the signal is passed through a PI estimator. The output of the PI estimator is the required change of resistance ΔR_s due to the change in temperature or frequency. The change of the stator resistance ΔR_s is continuously added to the previously estimated stator resistance $R_{s(k-1)}$. This updated stator resistance can be used directly in the controller.

VIII. Elimination of Voltage Sensors

In order to eliminate the dc offset of the voltage sensors, a simple method is introduced for estimating the phase voltages from the dc-link voltage and the inverter switching state ($\mathbf{S_a}$, $\mathbf{S_b}$, $\mathbf{S_c}$) [21]. However, the switching patterns in our practical setup are available in the complex programmable logic devices (CPLDs) that are applied to the PWM inverter with 1-μs resolution (as will be explained in Section XI). To solve this problem, the average voltages of each phase in each sampling interval (5 kHz) are computed using the sector number of the reference voltage space vector and timing assignment of the SVM-PWM inverter which are available in the PC. Depending on the sector number in which the inverter reference voltage vector is located in, the status of the upper switch of each leg is shown in Table I. S_a, S_b, and S_c refer to upper switch status of phases a, b, and c, respectively. Considering Table I, the average of the inverter phase voltages during sampling of T_s is obtained as

TABLE I
Upper Switch Status of Each Inverter Leg Based on Sector Number

Sector NO.	1		2		3		4		5		6	
	t_1	t_2	t_1	t_2	t_1	t_2	t_1	t_2	t_1	t_2	t_1	t_2
Sa	1	1	1	0	0	0	0	0	0	1	1	1
Sb	0	1	1	1	1	1	1	0	0	0	0	0
Sc	0	0	0	0	0	1	1	1	1	1	1	0

S_{ec1} *Matrix*

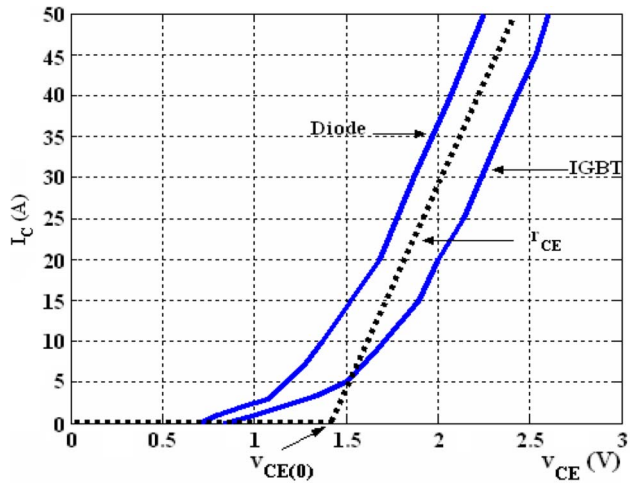

Fig. 4. Forward characteristics of the IGBT and diode of the power model.

$$\begin{pmatrix} v_{aN} \\ v_{bN} \\ v_{cN} \end{pmatrix} = \frac{V_{\rm dc}}{T_s} * S_{ec_i} * \begin{pmatrix} t_1 \\ t_2 \end{pmatrix}, \quad i = 1, \ldots, 6; \quad T_s = t_0 + t_1 + t_2 \tag{43}$$

where $V_{\rm dc}$ is the inverter dc-link voltage and "N" indicates the negative polarity of the dc link. t_1 and t_2 are the timing assignments, and $S_{{\rm ec}_i}$ is the ith sector matrix which is obtained from Table I. As an example, $S_{\rm ec1}$ is the first sector matrix

$$S_{\rm ec1} = \begin{pmatrix} 1 & 1 \\ 0 & 1 \\ 0 & 0 \end{pmatrix}. \tag{44}$$

Now, the components of space voltage in a two-axis stationary reference frame can be obtained as [22]

$$v_{\rm Ds} = 2/3 * (v_{aN} - 0.5 * v_{bN} - 0.5 * v_{cN}) \tag{45}$$

$$v_{\rm Qs} = 2/3 * (\sqrt{3}/2 * v_{bN} - \sqrt{3}/2 * v_{cN}). \tag{46}$$

One may note that zero time t_0 does not affect the components of the stator voltage space vector $(v_{\rm Ds}, v_{\rm Qs})$, and therefore, the status of the upper switch of each inverter leg during time t_0 is not shown in Table I and sector matrix.

IX. Effects of the FVD and its Compensation

At very low speed, the voltage drop in the PWM inverter can be higher than the induced voltage and hence constitutes a severe disturbance [23]. Fig. 4 shows the forward characteristics

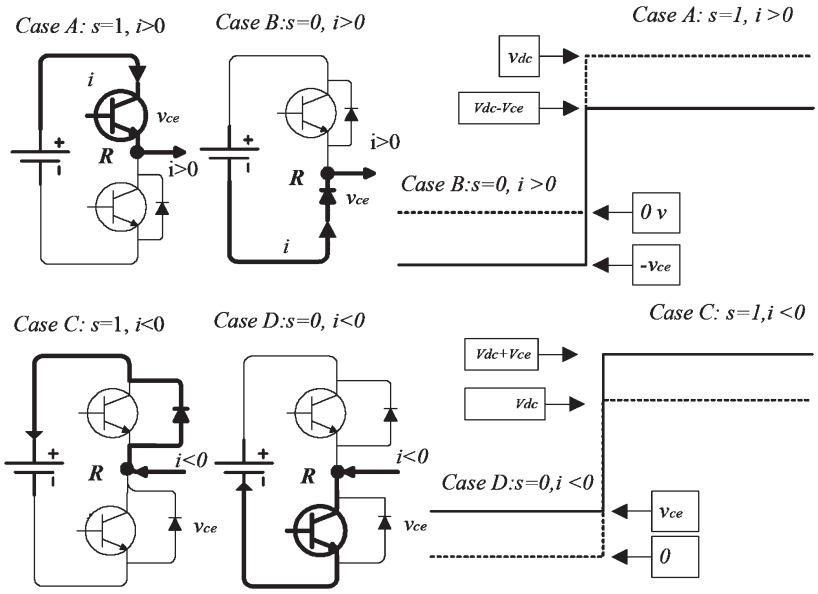

Fig. 5. Analysis of the output voltage of an inverter leg.

of the insulated-gate bipolar transistor (IGBT) and diode used in this project. It is well known that the forward characteristics of the IGBT and its freewheeling diode are nonlinear, and they vary with temperature. However, according to their forward characteristics shown in Fig. 4 and in the datasheet, both can be represented by a dc voltage source and a resistance, as shown in (47)

$$v_{\mathrm{CE}} = v_{\mathrm{CE0}} + ir_{\mathrm{CE}}. \tag{47}$$

In order to simplify the analysis, it is assumed that the forward voltage drops (FVDs) of the diode and the IGBT are the same. The resistance term in (47) can be assumed as an extra stator resistance and, therefore, could be estimated by the stator-resistance estimator mentioned in Section VII. In this section, the focus is on compensating the error caused by v_{CE0}.

The actual voltages with positive and negative currents are shown in Fig. 5. The left part of the figure is the inverter leg, the output voltage of which is either zero or V_{dc}, ideally. The letter "s" in Fig. 5 shows the switching function of the inverter leg. The output voltages of the inverter leg with positive current (into the load) and negative current (from the load) are compared under the conditions of $s = 1$ and $s = 0$. It is shown that, when the current is positive, the actual voltage is shifted down by v_{CE}; when the current is negative, the waveform of the actual output voltage of the inverter leg will be shifted up by v_{CE}. After circuit analysis of the inverter, the error caused by the FVD of the switches of the inverter can be found. The error caused by the FVD in one inverter leg can be shown in (48). Equation (49) shows the error vector of the inverter in the stationary frame

$$\Delta v_R = s * v_{\mathrm{DC}} - v_R = v_{\mathrm{CE0}} * \mathrm{sign}(i_R) \tag{48}$$

$$\Delta v = \frac{2}{3} v_{\mathrm{CE0}} * \left[\mathrm{sign}(i_R) + \alpha * \mathrm{sign}(i_S) + \alpha^2 * \mathrm{sign}(i_T)\right] \tag{49}$$

where $\mathrm{sign}(.)$ is signum function and $\alpha = e^{j2\pi/3}$.

Using (49), an estimated value $\hat{V}_s$ of the stator voltage vector can be obtained from the SV-PWM reference voltage vector v^* described as $\hat{V}_s = v^* - \Delta v$. Therefore, $\hat{\lambda}_s$ is corrected as

$$\hat{\lambda}_s = \int (v^* - \Delta v - \hat{R}_s i)\, dt + \lambda_0. \tag{50}$$

X. Experimental Setup and Results

The overall block diagram of the proposed drive system is shown in Fig. 6. In order to evaluate the performance of the actual system, a PC-based prototype system was built and tested. The experimental setup is shown in Figs. 7 and 8 and consists of the following sections: A 0.37-kW three-phase SynRM and a 1.1-kW dc generator as its load, a three-phase voltage source inverter and its isolation board, voltage and current sensors board, a 96-b Advantech digital input–output card, a 32-channel Advantech A/D converter card, a complex programmable logic device (CPLD) board, and a PC for calculating the required signals and viewing the registered waveforms. The 0.37-kW SynRM parameters are reported in Table II. The SynRM is supplied by a three-phase inverter with a symmetrical two-level space-vector modulation. A Xilinx XC95288xl CPLD has been selected for real-time implementation of switching patterns using a switching frequency of 5 kHz. The CPLD board communicates with the PC via the digital Advantech PCI-1753 I/O board. The CPLD in the experimental setup realizes the following tasks: switching pattern generation of the IGBT switches based on the SVM technique, providing a useful dead time in the so-called switching patterns of power switches, generation of the synchronizing signal for data transmission between the PC and the hardware, and shutting down the inverter in the case of emergency conditions such as overcurrent or PC hanging states. The inverter has been designed and implemented specifically for this experiment using an SKM75 GD 124 D SEMIKRON module. The required drive board has been designed by HCPL 316J, which is a fast and intelligent IGBT driver, and guarantees a reliable isolation between the

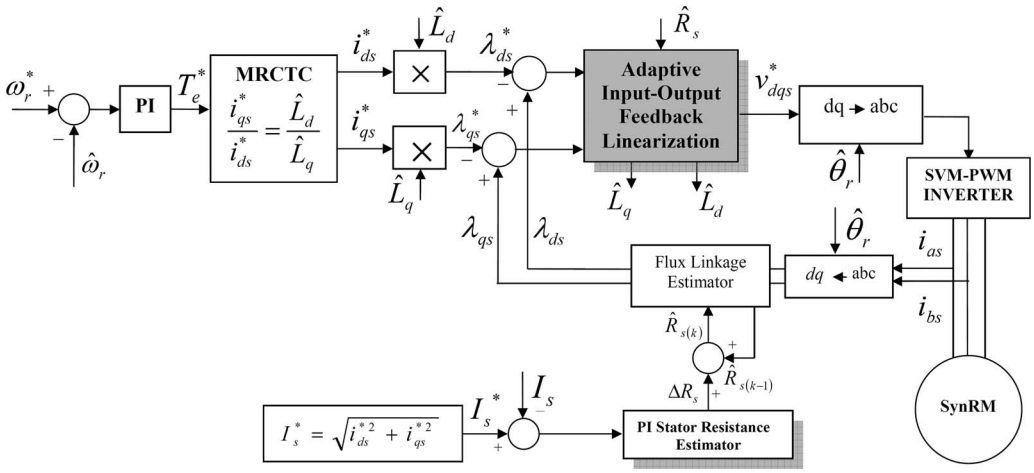

Fig. 6. Block diagram of SynRM drive system control.

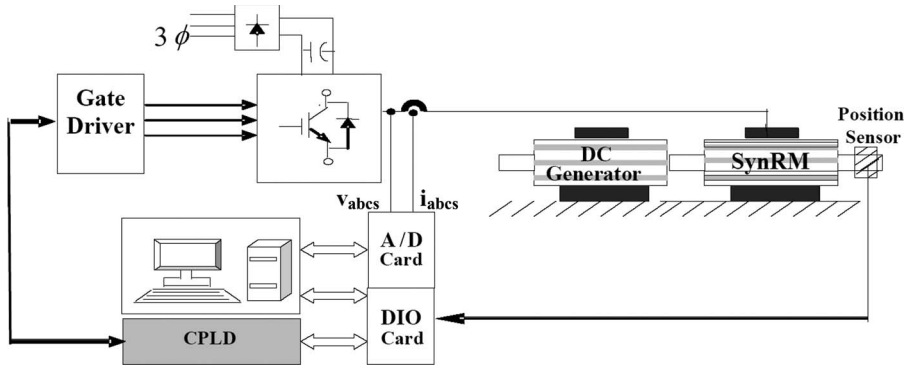

Fig. 7. Laboratory implementation block diagram.

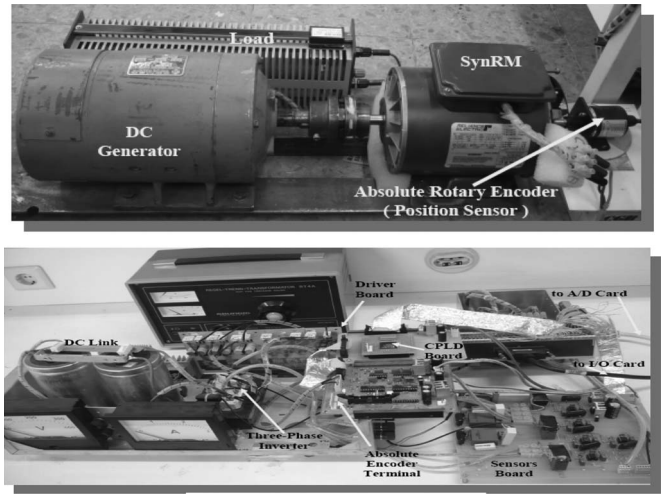

Fig. 8. Experimental setup.

high voltage and control boards. The dc-link voltage and the stator phase currents are measured by Hall-type LEM sensors. All measured electrical signals are filtered using the separate analog second-order low-pass filters with 1.5-kHz bandwidth and then converted to digital signals using an A/D card with 10-μs conversion time. In order to evaluate the accuracy of the rotor-speed and position estimation, the actual rotor position is obtained from an absolute encoder with 1024 pulses/r.

TABLE II
MOTOR NOMINAL CHARACTERISTICS

$P_n = 370\,W$	$V_n = 230$	$I_n = 2.8\,A$
$L_{md,un,Sat} = 232\,mH$	$L_{md,Sat} = 178\,mH$	$L_{mq} = 118\,mH$
$R_s = 2.95\,\Omega$	$f_n = 60$ Hz	No. of Poles: 4
$T_{en} = 1.9\,N.m$	$J_m = .015\,\text{Kg.m}^2$	$B_m = .003$ Nm/rad/sec
$L_{ls} = 10mH$	$L_{ldr} = 8\,mH$	$L_{lqr} = 12\,mH$
$R_{dr} = 2\,\Omega$	$R_{qr} = 2\,\Omega$	

In our proposed control approach, the system-controller gains are obtained by trial-and-error method, which are given by $K_P = 0.3$, $K_I = 0.05$, $\gamma_1 = 0.5$, $\gamma_2 = 3$, and $\alpha_1 = \alpha_2 = 225$. Assuming an exponential speed reference from 0 to 1000 r/min with rise time $\tau = 0.2$ s, the experimental results are obtained for the MRCTC strategy corresponding to a three-phase SynRM. The obtained results are shown in Figs. 9 and 11. As shown in Fig. 9, the desired torque is stepped up and stepped down in a time duration of 2.5 s. It is shown that, for a chosen i_d and i_q reference currents, the estimated values of L_d and L_q approximately converge to those that are obtained from Fig. 10, which shows the curves of L_d versus i_d and L_q versus i_q obtained by practical test. The performance of

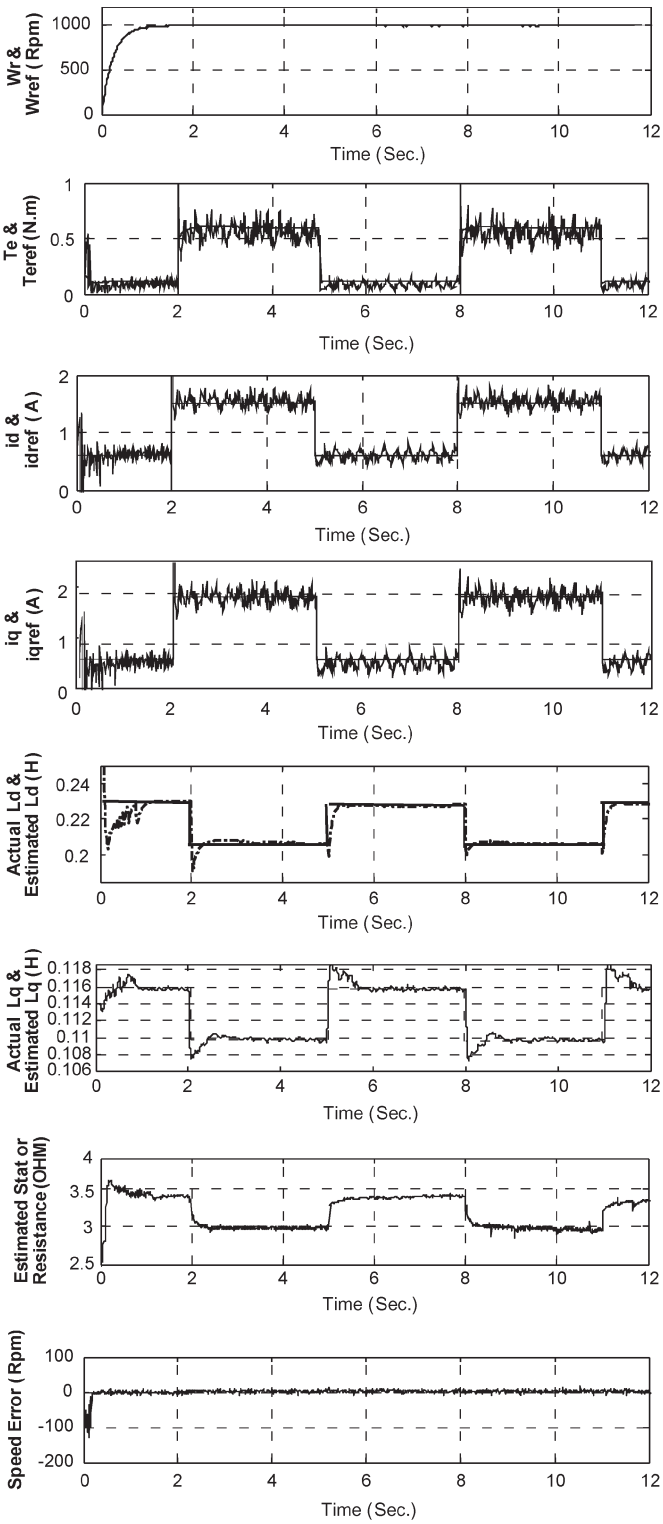

Fig. 9. SynRM MRCTC experimental results.

the proposed rotor-speed and position-estimation method at very low speed is shown in Fig. 11. The speed reference is reversed from $+10$ to -10 r/min at $t = 10$ s under 50% full load. It is seen that the reference speed is perfectly tracked and the position-estimation error could be suppressed within 4 electrical degrees. The torque and speed are smooth enough, and the flux hodograph is almost a circle.

XI. Conclusion

In this paper, an AIOFL controller has been designed for MRCTC of an encoderless three-phase SynRM drive. The controller is capable of simultaneous estimation of direct- and quadrature-axis inductances. It has been shown that, under PE condition, the estimation errors in the motor d- and q-axis

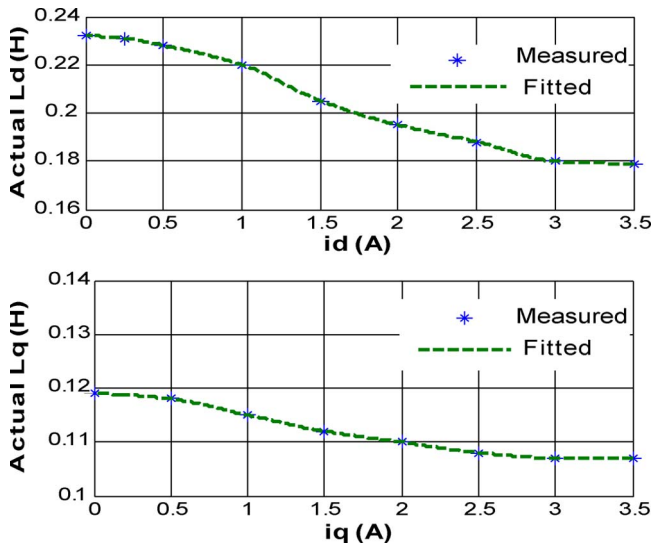

Fig. 10. Variation of d-axis inductance L_d versus d-axis current i_d and q-axis inductance L_q versus q-axis current i_q.

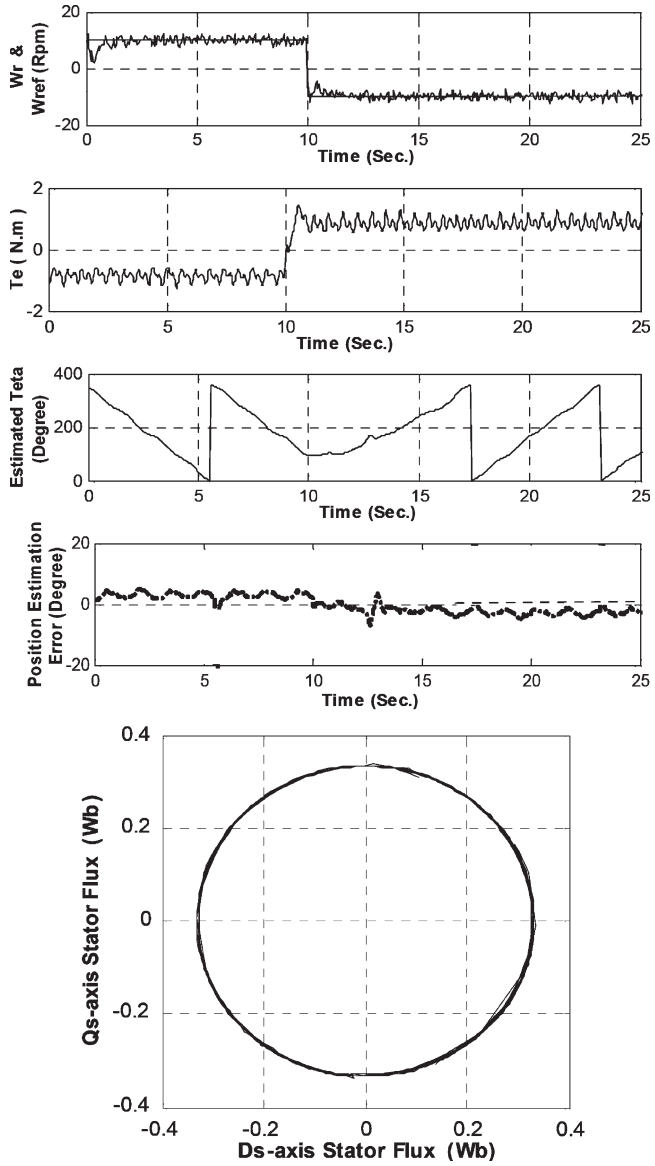

Fig. 11. Rotor low-speed and position estimation.

inductances asymptotically converge to zero. Based on this control approach, the rotor low-speed estimation has been achieved by using a simple method for eliminating the voltage sensors, a simple technique for online estimation of the stator resistance, and taking into account the FVD of the inverter power switches. Close agreement was observed between the results of the simulation and the experiment; any discrepancy between them is attributed to the limitations of the data acquisition system, and also to the motor iron loss that was not taken into account in the SynRM system model.

REFERENCES

[1] R. Morales-Caporal and M. Pacas, "A predictive torque control for the synchronous reluctance machine taking into account the magnetic cross saturation," *IEEE Trans. Ind. Electron.*, vol. 54, no. 2, pp. 1161–1167, Apr. 2007.

[2] T. H. Liu and H. H. Hsu, "Adaptive controller design for a synchronous reluctance motor drive system with direct torque control," *IET Elect. Power Appl.*, vol. 1, no. 5, pp. 815–824, Sep. 2007.

[3] H. F. Hofmann, S. R. Sanders, and A. EL-Antably, "Stator-flux-oriented vector control of synchronous reluctance machines with maximized efficiency," *IEEE Trans. Ind. Electron.*, vol. 51, no. 5, pp. 1066–1072, Oct. 2004.

[4] H. D. Lee, S. J. Kang, and S. K. Sul, "Efficiency-optimized DTC of synchronous reluctance motor using feedback linearization," *IEEE Trans. Ind. Electron.*, vol. 46, no. 1, pp. 192–198, Feb. 1999.

[5] P. Guglielmi, M. Pastorelli, and A. Vagati, "Impact of cross-saturation in sensorless control of transverse-laminated synchronous reluctance motors," *IEEE Trans. Ind. Electron.*, vol. 53, no. 2, pp. 429–439, Apr. 2006.

[6] A. Vagati, M. Pastorelli, and G. Franceschini, "High-performance control of synchronous reluctance motors," *IEEE Trans. Ind. Appl.*, vol. 33, no. 4, pp. 983–991, Jul./Aug. 1997.

[7] J.-D. Park, C. Kalev, and H. F. Hofmann, "Control of high-speed solid-rotor synchronous reluctance motor/generator for flywheel-based uninterruptible power supplies," *IEEE Trans. Ind. Electron.*, vol. 55, no. 8, pp. 3038–3046, Aug. 2008.

[8] A. Vagati, M. Pastorelli, F. Scapino, and G. Franceschini, "Impact of cross saturation in synchronous reluctance motors of the transverse-laminated type," *IEEE Trans. Ind. Appl.*, vol. 36, no. 4, pp. 1039–1046, Jul./Aug. 2004.

[9] K. M. Rahman and S. Hiti, "Identification of machine parameters of a synchronous motor," *IEEE Trans. Ind. Appl.*, vol. 41, no. 2, pp. 557–565, Mar./Apr. 2005.

[10] R. E. Betz, R. Lagerquist, and M. Jovanovic, "Control of synchronous reluctance machines," *IEEE Trans. Ind. Appl.*, vol. 29, no. 6, pp. 1110–1122, Nov./Dec. 1993.

[11] S. Ichikawa, M. Tomita, S. Doki, and S. Okuma, "Sensorless control of SynRMs based on extended EMF models considering magnetic saturation with online parameter identification," *IEEE Trans. Ind. Appl.*, vol. 42, no. 5, pp. 1264–1274, Sep./Oct. 2006.

[12] R. P. Marino, *Nonlinear Control Design*. Englewood Cliffs, NJ: Prentice-Hall, 1995.

[13] R. Morales-Caporal and M. Pacas, "Encoderless predictive DTC for SynRM at very low and zero speed," *IEEE Trans. Ind. Electron.*, vol. 55, no. 12, pp. 4408–4416, Dec. 2008.

[14] C. A. M. D. Ferraz and C. R. de Souza, "Considering iron losses in modeling the reluctance synchronous motor," in *Proc. 7th Int. Workshop AMC*, Jul. 2002, pp. 251–256.

[15] L. Tang and M. F. Rahman, "Investigation of an improved flux estimator of a direct torque controlled interior permanent magnet synchronous machine drive," in *Proc. 35th Annu. IEEE Power Electron. Spec. Conf.*, 2004, pp. 451–457.

[16] S. Mir, M. E. Elbuluk, and D. S. Zinger, "PI and fuzzy estimators for tuning the stator resistance in indirect torque control of induction machines," *IEEE Trans. Power Electron.*, vol. 13, no. 2, pp. 279–287, Mar. 1998.

[17] R. E. Betz, "Theoretical aspects of the control of synchronous reluctance machines," *Proc. Inst. Elect. Eng.*, vol. 139, no. 4, pt. B, pp. 355–364, Jul. 1992.

[18] R. E. Betz and T. J. E. Miller, "Aspects of the control of synchronous reluctance machines," in *Proc. EPE*, 1991, pp. 456–463.

[19] A. Chiba and T. Fukao, "A closed-loop operation of super high-speed reluctance motor for quick torque response," *IEEE Trans. Ind. Appl.*, vol. 28, no. 3, pp. 600–606, May/Jun. 1992.
[20] T. A. Lipo, "Synchronous reluctance machines—A viable alternative for ac drives," *Elect. Mach. Power Syst.*, vol. 19, pp. 659–671, 1991.
[21] J. Holtz and J. Quan, "Drift- and parameter-compensated flux estimator for persistent zero-stator-frequency operation of sensorless-controlled induction motors," *IEEE Trans. Ind. Appl.*, vol. 39, no. 4, pp. 1052–1060, Jul./Aug. 2003.
[22] V. D. Broeck, H. C. Skudelny, and G. V. Stanke, "Analysis and realization of a pulse width modulator based on voltage space vectors," *IEEE Trans. Ind. Appl.*, vol. 24, no. 1, pp. 142–150, Jan./Feb. 1988.
[23] J. Holtz, "Sensorless control of induction machines—With or without signal injection?" *IEEE Trans. Ind. Electron.*, vol. 53, no. 1, pp. 7–30, Feb. 2006.

Hossein Abootorabi Zarchi received the M.S. degree from Isfahan University of Technology, Isfahan, Iran, where he is currently working toward the Ph.D. degree with the Faculty of Electrical and Computer Engineering.

He is a Visiting Ph.D. Student with the Control and Automation Group, Denmark Technical University, Denmark, from May 2009 to February 2010. His research interests are nonlinear control, fault diagnosis in electromechanical systems, power electronics, and variable-speed ac drives.

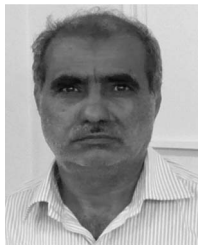

Jafar Soltani graduated from Tabriz University, Tabriz, Iran, and received the M.S. and Ph.D. degrees from the University of Manchester Institute of Science and Technology, Manchester, U.K.

He is currently an Emeritus Professor with the Faculty of Electrical and Computer Engineering, Isfahan University of Technology, Isfahan, Iran. His main area of research is on electrical machines and drives. He has published many international journal and conference papers and is the holder of a U.K. patent.

Dr. Soltani is a member of the Institution of Engineering and Technology.

Gholamreza Arab Markadeh received the M.S. and Ph.D. degrees from Isfahan University of Technology, Isfahan, Iran.

He is currently an Assistant Professor in the Department of Engineering, Shahrekord University, Shahrekord, Iran. His main areas of research are nonlinear control, power electronics, and variable-speed ac drives.

Mark	Rank	Abbreviated Journal Title	ISSN	JCR Data						EigenfactorTM Metrics		JCR©2009 Impact Factor Regenerated by Jones
				Total Cites	Impact Factor	5-Year Impact Factor	Immediacy Index	Articles	Cited Half-life	Eigenfactor™ Score	Article Influence™ Score	
	1	4OR-Q J OPER RES	1619-4500	130	0.75		0	31	4.2	0.00125		
	2981	IEEE GEOSCI REMOTE S	1545-598X	979	1.379		0.16	175	3.1	0.00798		
	2982	IEEE IND APPL MAG	1077-2618	455	0.727	0.684	0.109	46	7.5	0.00137	0.305	
	2983	IEEE IND ELECTRON M	1932-4529	62	1.75	1.75	0.235	17		0.00042	0.633	
	2984	IEEE INSTRU MEAS MAG	1094-6969	218	0.738	0.736	0.25	32	5.3	0.00074	0.224	
	2985	IEEE INTELL SYST	1541-1672	2214	3.144	3.594	0.333	33	6.5	0.00447	0.763	

باسمه تعالی

تاریخ: ۱۴۰۱/۳/۲۳

فرم خود ارزیابی مقاله ژورنالی

(توسط متقاضی)

همکار ارجمند

با توجه به اهمیت داوری صحیح مقاله ها، خواهشمند است به پرسش های زیر با دقت پاسخ دهید. همچنین، گزارش طرح های پژوهشی، پایان نامه کارشناسی ارشد و رساله دکتری خود را به ضمیمه مدارک تسلیم دارید. درخواست می شود لطفا به همپوشانی آثار، توجه ویژه ای مبذول فرمایید.

شماره ردیف: 2 **عنوان مقاله: (با ۱۰۰ ارجاع)**

Adaptive Input–Output Feedback-Linearization-Based Torque Control of Synchronous Reluctance Motor without Mechanical Sensor

۱- آیا مقاله ای با محتوای مشابه در جای دیگری چاپ شده است؟ خیر ■ آری☐ نمی دانم☐

۲- آیا این مقاله با مقاله های دیگر شما همپوشانی دارد؟ (*به مانند: روش حل، نتایج و ...*) خیر ■ آری☐ درصد همپوشانی:

شماره ردیف مقاله: عنوان مقاله‌ای که همپوشانی دارد:

۳- درجه علمی مجله علمی پژوهشی معتبر (JCR , Scopus – علمی پژوهشی داخلی) که مقاله در آن منتشر شده است:

عالی■ بسیار خوب☐ خوب☐ متوسط☐ ضعیف☐

٤- محتوای مقاله از نظر ویژگی های زیر چگونه است؟

۱-اعتبار علمی: عالی■ خوب☐ متوسط☐ ضعیف☐

۲- نوآوری و ابتکار: عالی■ خوب☐ متوسط☐ ضعیف☐

۵- آیا مقاله مستخرج از پایان نامه‌ی کارشناسی ارشد و یا از رساله‌ی دکترای جنابعالی می باشد؟

خیر ☐ آری■ درصد همپوشانی:100%

در صورتی که پاسخ به سؤال بالا مثبت باشد، به پرسش های زیر پاسخ فرمایید:

الف- فرض های به کار رفته و محتویات اصلی تا چه حد بر موارد همانند در پایان نامه و یا رساله منطبق است؟

ب- آیا روش تحلیل و یا نتیجه گیری با موارد همانند در پایان نامه و یا رساله مشابهت دارد؟

٦- آیا این مقاله با مقالات کنفرانسی شما همپوشانی دارد؟

خیر■ آری☐ میزان درصد همپوشانی:

شماره ردیف مقاله: عنوان مقاله‌ای که همپوشانی دارد:

۷- آیا این مقاله با طرح های پژوهشی یا طرح اینترنشیپ شما همپوشانی دارد؟ خیر■ آری☐ درصد همپوشانی:

عنوان طرح:

۸- آیا مقاله (برای استادی شما) با مقالات دانشیاری شما همپوشانی دارد ؟ خیر■ آری☐ درصد همپوشانی:

عنوان مقاله‌ای که همپوشانی دارد:

لطفاً چنانچه نظر اصلاحی یا تکمیلی دارید در این صفحه یا در پشت برگه درج فرمایید.

حسین ابوترابی زارچی

امضاء